ELSEVIER

Surface Science 505 (2002) 93–114

SURFACE SCIENCE

www.elsevier.com/locate/susc

Surface oxygenation studies on (1 0 0)-oriented diamond using an atom beam source and local anodic oxidation

K.P. Loh [a,*], X.N. Xie [a], Y.H. Lim [a], E.J. Teo [b], J.C. Zheng [b], T. Ando [c]

[a] *Department of Chemistry, National University of Singapore, 3 Science Drive 3, Lower Kent Ridge Road, Singapore 117543, Singapore*
[b] *Department of Physics, National University of Singapore, Lower Kent Ridge Road, Singapore 119260, Singapore*
[c] *National Institute for Material Science, 1-1 Namiki, Tsukuba-shi, Ibaraki 305-0044, Japan*

Received 9 August 2001; accepted for publication 14 November 2001

Abstract

Surface oxidation studies on pre-deuterated (1 0 0)-oriented single crystal diamond have been performed by oxidizing the diamond surfaces macroscopically using an oxygen atomic beam source as well as microscopically using local anodic oxidation by atomic force microscope (AFM). Oxygen-deuterium exchange on diamond (1 0 0) was investigated by X-ray photoelectron spectroscopy, elastic recoil detection and time-of-flight SIMS. Exchange of pre-adsorbed D by atomic O is thermally activated, with almost complete exchange of surface D by atomic O at 300 °C. At higher oxidation temperatures, oxidation states which are chemically shifted from the C 1s bulk peak by 3.2 eV was observed together with a disordering of the diamond surface. Micron-scale, localized oxygenation of the diamond surface at room temperature could be achieved with a biased AFM tip where we confirmed that the modified areas show a lower secondary electron yield and higher oxygen content. In addition, the electronic structure of the oxygenated diamond surface (on-top (OT) and bridging model) has been investigated by calculating the layered-resolved partial density of states using first principles plane wave ab initio pseudopotential method within the local density functional theory. For the oxygen OT model, sharp features due to occupied surface states in the valence band and unoccupied surface states in the gap exist. The increase in emission intensity near the valence band edge for oxygenated diamond (1 0 0) was verified by ultraviolet photoelectron spectroscopy study.

Keywords: Diamond; Oxidation; Atomic force microscopy; Chemisorption

1. Introduction

The chemistry of oxygen chemisorption on diamond surfaces and the electronic properties of oxygenated diamond present a rich area for fundamental surface science studies [1–7]. Controlled oxygenation of single crystal diamond to produce a well-defined, smooth oxygenated surface is interesting from both fundamental and technological perspectives. In contrast to silicon, the oxygenated diamond interface is limited to a monolayer (ML) even at high-pressure or high-temperature oxidation conditions. The ultrathin, oxygenated interface imparts distinctive electronic and physical properties to the diamond. The oxygenated diamond surface is hydrophilic, has a positive electron affinity and a low surface

* Corresponding author. Tel.: +65-874-4778; Fax: +65-779-1691.
E-mail address: chmlohkp@nus.edu.sg (K.P. Loh).

0039-6028/02/$ - see front matter
PII: S0039-6028(02)01103-2

conductivity. In contrast, the hydrogenated diamond surface is hydrophobic and exhibits negative electron affinity (NEA) and low resistivity [8]. By creating spatially resolved oxygenated and hydrogenated domains on the diamond surface, a special type of lateral transistor which utilizes the property of surface conductivity at the gate for controlling the tunneling barrier height has been demonstrated recently [9,10]. On the other hand, desirable surface properties of the hydrogenated diamond such as NEA and surface conductivity are easily corrupted by oxygen and limit the application of diamond as photocathodes [11] and electrodes. Introducing oxygen into the chemical vapor deposition (CVD) gas feed has been known to promote deposition of high quality crystalline diamond films at lower temperature, prompting questions about the role of oxygen during diamond CVD [12].

The controlled uptake of oxygen on the diamond surface, or procedures for the effective exchange of surface chemisorbed oxygen with hydrogen, or vice versa, has not been established clearly. Molecular oxygen shows no appreciable sticking probability on diamond in vacuum, but moisture may cause a slow oxidation of the surface under ambient conditions. Oxidation can be effected by subjecting the diamond to high-temperature treatment in an oxygen flow tube at high pressure [13]. The difficulty in preparing a well-characterized oxygenated surface stems from the very facile etching and roughening of the diamond surfaces at high temperature. It is desired to search for a less vigorous route for the oxygenation of diamond surface so that the surface structure of the diamond can be maintained for surface science investigation. Pehrsson et al. had examined in detail the oxidation chemistry of hydrogenated C(1 0 0) by activating molecular oxygen over an iridium filament and observed peroxy, carbonyl, ether and hydroxyl groups on the surface, pointing to the complexity of the co-adsorbed hydrogen/oxygen C(1 0 0) system [1,2]. However the filament activation method produces thermally excited O_2 rather than atomic O, and caution has to be exercised to control the filament temperature to prevent the evaporation of metal oxides on the surface. Recently we reported that atomic oxygen beam treatment of the surface using a radio-frequency atom beam source in high vacuum constitutes an efficient route to generate an oxidized diamond surface without destroying the surface structure [14]. In this work, we directly probe for the efficiency of O–D exchange on pre-deuterated diamond by performing ERDA, time-of flight SIMS (TOF-SIMS) and high resolution XPS. Besides macroscopic oxidation with the atom beam source, we have also researched on microscopic oxidation of the diamond surface to investigate whether low temperature, controlled oxidation of the diamond could be performed under ambient conditions.

Theoretical studies of clean and hydrogenated diamond (1 0 0) surfaces have been performed using various empirical and semiempirical techniques with the level of sophistication ranging from slab-MINDO [15], empirical tight binding methods [16,17] to non-self-consistent local density functional (LDF) calculations [18,19]. However the electronic structure of oxygenated diamond has received little attention. Previously we have calculated the density of states (DOS) on diamond (1 0 0) previously using first principles linear muffin-tin orbital (LMTO) method [14] and showed that distinct oxygenated states exist in the valence band for oxygenated diamond (1 0 0). In this study, the more sophisticated ab initio calculations were performed to consider the detailed layered projection DOS.

2. Experimental

The experiments were carried out in a UHV chamber equipped with surface analysis facilities such as UPS, XPS and RHEED. A 13.56 MHz RF plasma atom beam source was installed in the same chamber such that the surface modification of the diamond samples could be studied in situ using these analysis techniques. The sample used was a semiconducting diamond single crystal ($4 \times 4 \times 0.5$ mm^3) grown homoepitaxially on synthetic diamond (1 0 0) face by microwave enhanced CVD. The diamond crystal was mounted on a SiC backing plate clamped onto a azimuthally rotatable Mo sample holder. The sample could be

heated to 1200 °C by thermal conduction from the resistively heated SiC backing plate as verified by a thermocouple attached to the diamond sample face. UPS data was collected in the normal emission using He I excitation from a noble gas discharge lamp. RHEED was performed using a differentially pumped electron gun with the beam energy fixed at 25 keV. A remote discharge RF atomic beam source was used to generate atomic beams of D or O species from the parent molecular gases with the discharge zone operating typically at 300 W. We had applied optical emission spectroscopy to monitor for the presence of O_2^+ or O^* species in our RF-plasma O discharge. Spectral lines due exclusively to the I lines of excited atomic O at 777.2 (strongest), 645.5, 615.8, 543.6, 532.9, 436.8 and 394.7 nm were detected, whilst no O_2^+ spectral lines (559.8 nm) was observed, testifying that the atomic beam source produced predominantly atomic O (excited and ground state species). The radicals then effused from a capillary effuser onto the sample face, mounted about 2 cm away. The chamber pressure was maintained at 1×10^{-3} Torr during the operation of RF discharge and recovered to 1×10^{-9} Torr within 10 min after use. Typically, samples that would be examined by ex situ techniques such as ERDA and TOF-SIMS were introduced into the analysis chamber within two hours of their treatment by plasma to minimize contamination.

ERDA was performed in the Research Centre for Nuclear Microscopy at the National University of Singapore, using a HVEC 2.5 MV ion accelerator and a OM2000 high-excitation triplet quadrupole lens system. A 2.0 MeV He ion beam with an incident angle of 77° with respect to sample normal and with a beam size of 1×1 mm^2 was used for the analysis. The ERDA detector was located at a recoil angle of 30°. The experimental ERDA spectra were calibrated and simulated using SIMNRA program (version 7.0). The deuterium peak was accurately identified and quantified. The base pressure of the chamber was 1×10^{-7} Torr.

Ultra-shallow depth profiling of the deuterated diamond surface was performed using a Cameca IONTOF system equipped with dual pulsed ion beam operating in the interlaced mode. The base pressure of the system was 1×10^{-9} Torr. A pulsed keV Ar gun was used for sputtering and a 25 keV Ga gun was used for analysis. The sputtering area $= 300 \times 300$ μm^2 and the analysis area $= 50 \times 50$ μm^2.

The atomic force microscope (AFM) work in this study was performed using a Picoscan system (Molecular Imaging Co., Phoenix, AZ) with conducting silicon tips prepared by sputtering nickel on the tip.

3. Results

3.1. Oxidation studies on diamond (100)

A clear $2 \times 1/1 \times 2$ reconstruction could be observed on the deuterium-terminated diamond surface prepared by post-treatment of the as-grown diamond by RF-deuterium plasma beam. The RF-deuterium plasma beam was applied at a glancing incidence to facilitate the surface polishing. Preliminary experiments looked at the transformation in the RHEED pattern on the smooth $2 \times 1/1 \times 2$ deuterium-terminated diamond after being irradiated with atomic O beam source for different lengths of time. The $2 \times 1/1 \times 2$ face as shown in Fig. 1(a) is characterized by the appearance of a clear half-order ring of spots between the zero Laue zone and first-order Laue zone. The spacing between the streaks in $L_{1/2}$ has a separation which is consistent with a double domain $2 \times 1/1 \times 2$ (abbreviated here as 2×1). This diffraction pattern occurs on the (1 0 0) diamond surfaces when monolayer-high steps are present to give two orthogonal (2×1) domains [20]. Exposing the above surface to O-plasma beam at room temperature (RT) caused the intensity of the 2×1 diffraction beams to weaken, but the 2×1 reconstruction did not disappear totally even after 30 min of exposure. If the temperature of the substrate was increased to 300 °C during the O-plasma beam treatment, the 2×1 reconstruction was readily lost and a sharp 1×1 RHEED pattern was obtained, as shown in Fig. 1(b). Annealing the sample to 800 °C recovered the 2×1 pattern, even though the sharpness of the 2×1 pattern decreased after several cycles of oxygen-plasma treatment and annealing. If the O-plasma treatment was

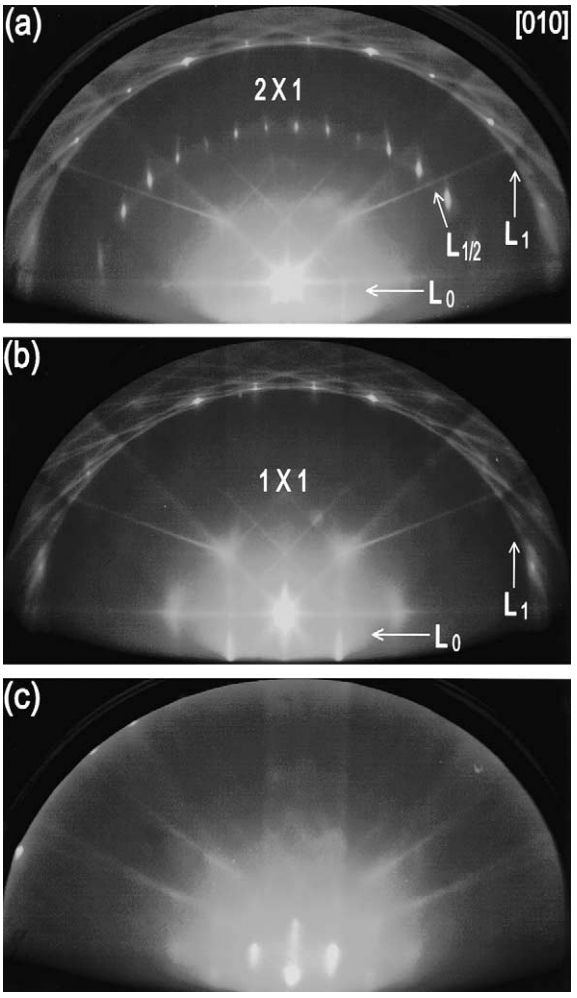

Fig. 1. (a) RHEED pattern taken in the [0 1 0] azimuth following glancing-angle RF D-plasma beam etching for 20 min. (b) RHEED pattern after O-atom beam treatment, substrate temperature: 300 °C, time: 10 min. (c) Substrate temperature: 500 °C, time: 10 min.

increased to 500 °C, the surface became rough as can be judged by the spotty appearance in the RHEED pattern shown in Fig. 1(c), in such a situation, the 2×1 pattern could not be recovered.

Monochromatised XPS was used to investigate the changes in the C 1s core level line shape with increasing uptake of O on the surface. Below an oxidation temperature of 400 °C, the uptake of oxygen was limited to a monolayer. The signature of monolayer oxidation is a narrow C 1s peak (FWHM = 1.2 eV) situated at 284.5 eV, and coexisting with a small shoulder at 285.8 eV, as shown in Fig. 2. This small shoulder could be attributed to carbonyl or ether type species. Following higher oxidation temperatures, a chemically shifted component near 287.5 eV increased in intensity with temperature, along with a broadening of the C 1s FWHM peak, suggesting the presence of multiple oxygen binding states on the surface. The ~3.2 eV chemically shifted component should be related to higher oxidation state species such as carboxylic or anhydride [21]. Increasing the treatment temperature to higher than 400 °C resulted in roughening of the diamond surface and degradation of the diamond crystallinity, as reflected by the increase in FWHM of the C 1s line to more than 2 eV from the initial 1.2 eV,

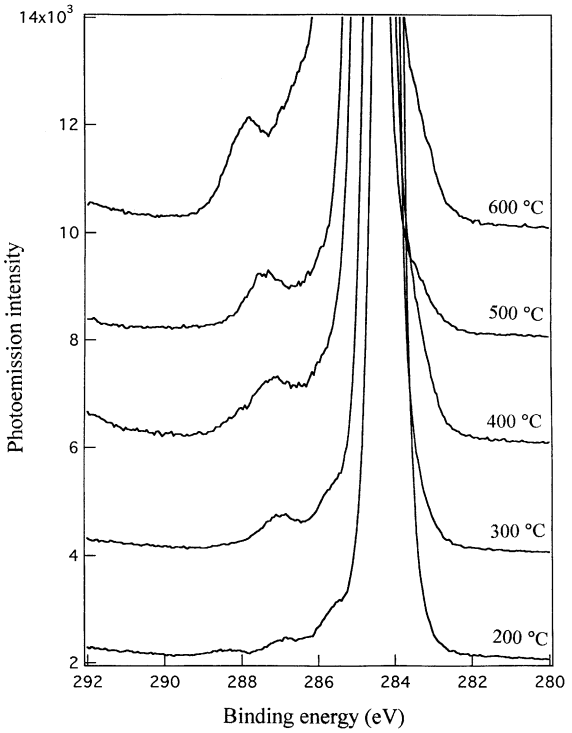

Fig. 2. XPS showing the C 1s core level following O-plasma beam treatment of the D-plasma pre-treated diamond at different indicated temperatures. Note the growth of the chemically shifted components as well as the increase in FWHM of the C 1s peak with increasing oxidation temperature.

although it was at this point where the highest concentration of bound oxygen species was detected. The increase in faceting and defects at higher temperature may promote the formation of carboxylic species on the surface and increase the surface oxygen coverage [2].

To establish whether the O atomic beam treatment is effective in removing the surface deuterium on the surface, a ''deuterium'' sensitive probe has to be applied. A priori, it is difficult to know the aerial density of D on the surface after O beam treatment since electron spectroscopic techniques cannot detect D(H). Quantification by vibrational loss techniques such as HREELS is difficult because electron scattering process is complex and influenced by sample conductivity and surface roughness. Yagi et al. [22] have investigated by ERDA and RBS the hydrogen and oxygen density on C(1 0 0) surface but no mapping of the aerial densities of the chemisorbed D (or H) after O-plasma treatment has been performed.

We employed the technique of ERDA to compare the surface deuterium content on three D-plasma treated diamond samples following O-plasma beam treatment at 25, 300 and 500 °C for the same treatment time. For a fully deuterated surface prepared by RF-deuterium plasma treatment, the deuterium concentration has been determined at first to be about 2.5×10^{15} atoms/cm^2, which is 1.5 times the surface atom density of an ideal C(1 0 0) surface. The deviation from ideal coverage is expected due to the presence of steps and defects on the real surface which have a higher adsorption area for D [22]. The deuterated samples have been verified by RHEED to exhibit air-stable D:C(1 0 0) 2×1 reconstruction after D-plasma treatment at 800 °C, although it has to be acknowledged that the air stability of the partially oxygenated surface is unknown. Nonetheless, a clear trend indicating a decline in surface D content of the sample is obtained with higher temperature treatment of oxygen-plasma treatment.

The elastic recoiled peaks of D are shown in Fig. 3(a). We can clearly see a decrease in the intensity of D peak at high oxidation temperature. For the sample treated with atomic O beam at 25 °C, the D aerial density was determined to be 0.9×10^{15} atoms/cm^2. Since the atom density of an ideal C (1 0 0) surface is 1.6×10^{15} atoms/cm^2, the above coverage corresponds to a surface coverage of 0.56 ML. For a second sample that was subjected to atomic O beam at 300 °C, an aerial density of 3.6×10^{14} D atoms/cm^2 (0.23 ML) was obtained. The D counts of the third sample which was treated with atomic O beam at 500 °C is almost at the noise level (2×10^{13} D/cm^2), indicating a complete exchange of chemisorbed D by O. A corresponding increase in the recoil signal of the oxygen peak is seen with the decrease in the D signal, indicating direct replacement of the surface D by O at higher treatment temperatures. A saturated intensity of $\sim 1 \times 10^{15}$ O atoms/cm^2 was obtained following O atom beam treatment at 300 °C.

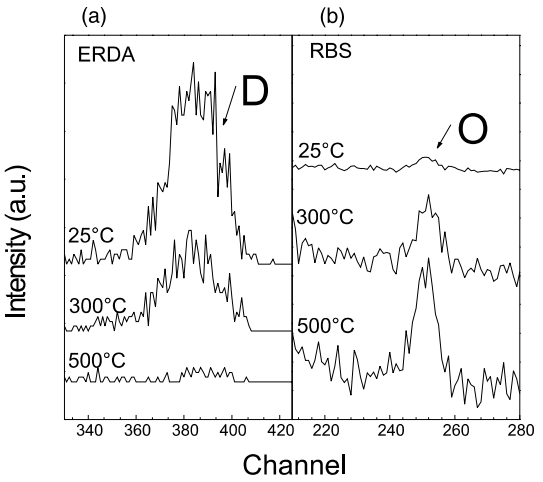

Fig. 3. ERDA spectra showing (a) the changes in D recoil signals for three samples that have been treated with O-atom beam at different temperatures and (b) the corresponding recoiled O signal. The increase in recoiled O signal mirrors the decrease in recoiled D signal.

The negative ion depth profile acquired by TOF-SIMS of two separate pre-deuterated diamond surfaces exposed to atomic O beam at 25 and 300 °C are displayed in Fig. 4(a) and (b). The mass resolution in this experiments was 5000 at 29 atomic mass unit, so secondary ions with nearly similar m/e values, such as H_2^- ($m/e = 2.020$) and D^- ($m/e = 2.015$), O^- ($m/e = 16.000$) and CD_2^- ($m/e = 16.040$) could be resolved. The main negative secondary ion species detected were D^-, O^-, OD^-, CD^-, CO^- ions, bigger cluster ions such as

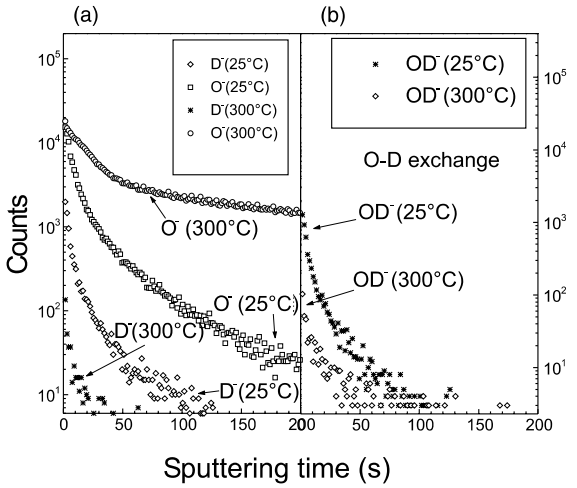

Fig. 4. (a) TOF-SIMS spectra showing the intensities of O^- and D^- for pre-deuterated diamond exposed to O-plasma beam for 15 min at RT and 300 °C and (b) corresponding TOF-SIMS spectra monitoring OD^- species.

CD_2^- and CD_3^- were not observed. As can be seen in Fig. 4(a), the intensity of D^- for the sample treated with atomic O beam at RT exhibits a rapid decay within the first 90 s, while the drop of O^- intensity is relatively slower due to its higher negative secondary ion yield and background contribution. For the sample that was treated with atomic O at 300 °C, the D^- intensity drops abruptly to zero within the first 25 s, while the O^- intensity increases by two orders of magnitudes at the equilibrium region compared to the sample treated at 25 °C. In Fig. 4(b), the depth profile of OD^- shows a similar trend for both except the initial intensity for the sample subjected to O atom beam treatment at 25 °C is one order of magnitude higher than that treated at 300 °C. No D^- signal could be detected for a third sample subjected to O atom beam treatment at 500 °C so the results are not shown here. In the cluster ion emission model [23], it is suggested that the emitted dimer species originate from the next-nearest neighbour in the local surface structures rather than a recombination of distant atoms emitted separately from different sites. Therefore, the observation of ions such as CD^-, CO^-, OD^- indicates the presence of C—D, C—O, and O—D bonds on the O—D exchanged C(1 0 0) surfaces.

The effect of O atom beam treatment on the valence band structure was investigated by studying the spectral transformation in the UPS He (I) spectra of the 2×1 deuterated diamond with O uptake. Uptake of 0.2 ML of O is sufficient to attenuate fully the sharp final-state emission peak at the low kinetic energy end, as shown in Fig. 5(a)-(i)–(iii). The sharp peak is the well-known NEA peak of diamond and is brought about by a lowering of the vacuum level beneath the conduction band minimum (CBM) [8]. The NEA condition facilitates the barrier-free escape of CBM electrons. Less than a monolayer of oxygen is sufficient to effect a conversion of the NEA condition on the deuterated surface to a positive electron affinity condition. For a surface that has been subjected to longer O-beam treatment time, there is an increase in valence band emission intensity between 0 and 4 eV, as shown in Fig. 5(iii). We rule out the possibility that this intensity increase is a consequence of the increase in the density of p–π states on the diamond surface due to ion irradiation effects because this emission state vanishes with the desorption of O from the surface, this is shown in the series of spectra in Fig. 5(b)-(i)–(v). In fact, we will show later in our total DOS (TDOS) calculations, that feature is consistent with oxygen-induced surface states. Fig. 5(b)-(i)–(v) shows the change in the spectral features when the oxygenated diamond was annealed to successively higher temperature. The enhanced emission feature between 0 and 5 eV was observed to reduce in intensity along with a shift of vacuum cut-off to higher binding energies. A change of the surface work function by ~2 eV between the oxygen-terminated and oxygen-free surface can be judged from the movement of the vacuum cut-off. In (iv), following the desorption of O from the surface at 700 °C, the secondary electron yield has recovered to a certain extent, although its intensity is only a fraction of the original NEA peak, suggesting that much of the surface chemisorbed D responsible for NEA has been replaced by atomic O. In (v), following the annealing of the surface to 850 °C, a peak near the Fermi level emerges, this feature accompanies the transition of the 1×1 surface structure to 2×1 and is due to the reconstruction of the sub-surface carbon layer fol-

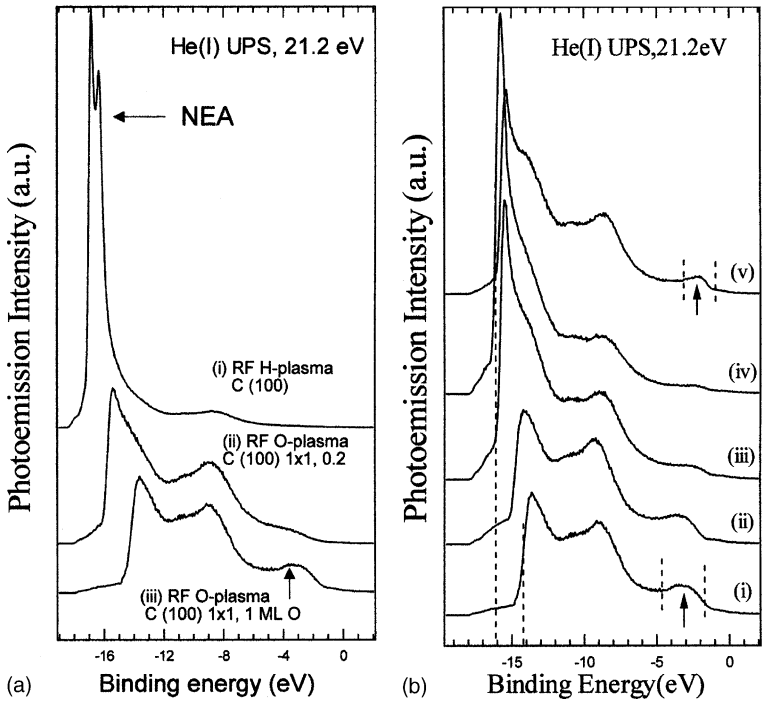

Fig. 5. (a) UPS He (I) spectra for diamond (1 0 0): (i) H:C(1 0 0) 2 × 1, showing strong characteristic NEA peak at 16.7 eV; (ii) O:C (1 0 0) 1 × 1, prepared directly from (i) by exposing it to O-plasma beam for 3 min at RT; (iii) an increase in emission intensity between 0 and 4 eV is visible following further oxygenation at 300 °C. (b) UPS spectra showing the changes when (i) oxygenated diamond (1 0 0) 1 × 1 was annealed to successively higher temperatures at (ii) 300 (iii) 500 (iv) 700 and (v) 850 °C. Note the emergence of the surface state peak at 2.5 eV after the attenuation of the O-related surface state peak at 3 eV.

lowing the desorption of O from the surface as CO or CO_2 species, with the ultimate generation of a clean C(1 0 0) 2 × 1 surface. Our DOS calculations in the following sections also reveal the emergence of a surface state due to the p–π bondings of the surface dimer atoms on the clean C(1 0 0) 2 × 1 face.

Microscopic oxidation of the pre-hydrogenated diamond surface using local anodic oxidation was attempted with a conducting AFM tip in air. Tip-induced anodic surface oxidation on silicon is known to be controlled by the density of water molecule in the air and the production of O anions from the ambient humidity [24]. Previous attempts on diamond was attempted by Tachiki et al. [9] using the constant height mode of AFM but no direct verification of the chemical composition of the modified area was obtained due to the limited spatial resolution of their technique.

Fig. 6(a)–(f) shows the AFM images of the modified diamond (1 0 0) surface collected in constant height, constant force and lateral force mode after line scanning at a 200 nm/s scan rate with the application of different sample bias in air. Strips of about 1000 nm^2 were fabricated on areas showing a bright contrast. In the topographic mode, the enhanced brightness translates to a measured height change of 4–5 nm on a surface with an average roughness of 0.6 nm. The parallel array of strips with different contrast were fabricated by stepping down the sample bias from 8 to 4 V, achieving a graded modification of the surface. The best possible contrast was achieved when a 8 V sample bias was applied. In the lateral friction mode, as shown in Fig. 6(c) and (f), the modified area exhibits a higher lateral friction compared to the unmodified area. This can be explained by the higher shear force experienced by the AFM tip on

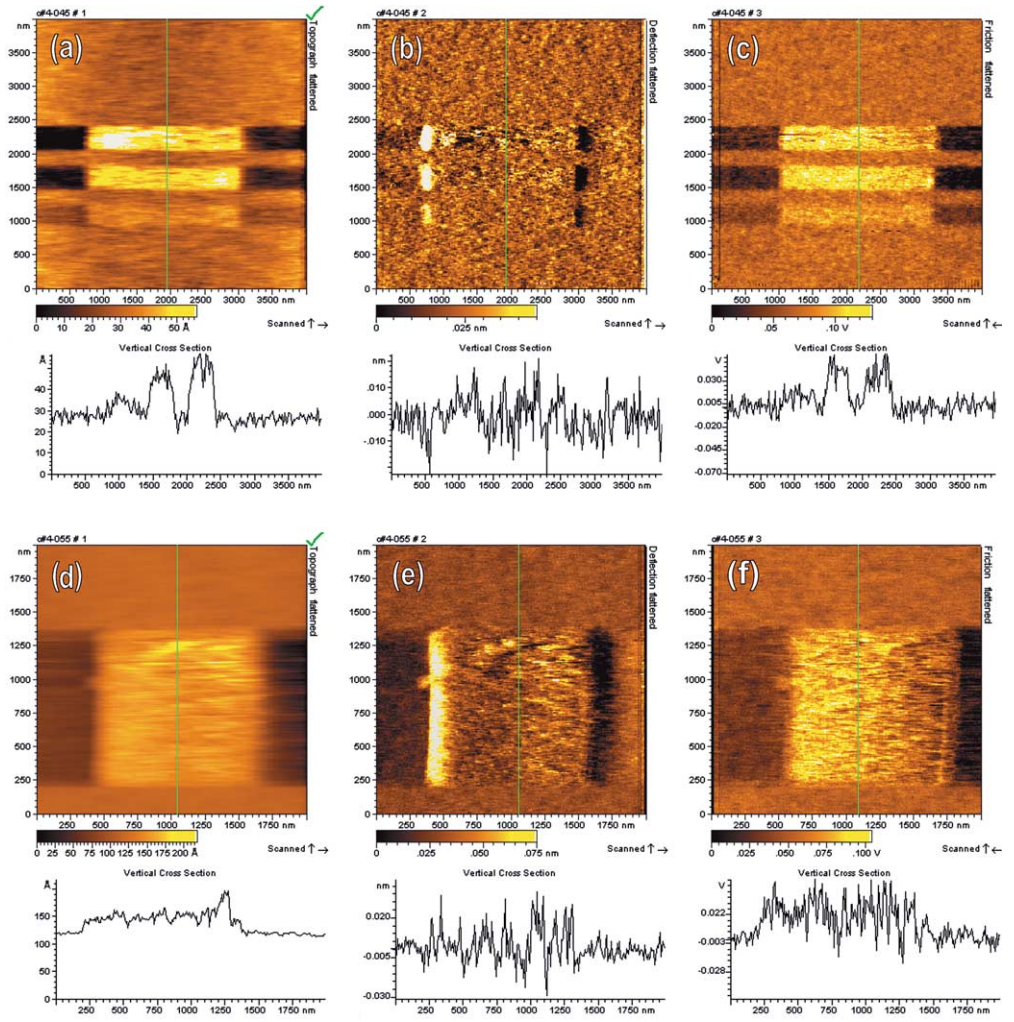

Fig. 6. (a–c) AFM image showing stark contrast between areas subjected to local anodic oxidation (brighter) and the non-modified areas (darker) collected at the constant height, constant force and lateral force mode respectively. The graded contrast of the different strips was obtained by varying the substrate bias from +8, 7 to 6 V. (d)–(e) Similar but showing a square, the best contrast was obtained using the lateral friction mode.

the C—O terminated surface compared to C—H terminations, due to the more polar character of the former. The scanning electron micrograph of the modified square as shown in Fig. 7 is distinguished by an area of lower secondary electron yield, which is characteristic of the positive electron affinity oxygenated area. Scanning auger microprobe analysis reveals that the modified area (1×1 μm^2) has a higher content of O compared to the surrounding regions, as shown in Fig. 7(a). To investigate the effect of substrate temperature on the ease of achieving local modification, the modification was performed with the substrate held at RT, 40 and 100 °C respectively. The cross-sectional height profile in Fig. 7(b)–(d) shows a corresponding decrease in the height of the modi-

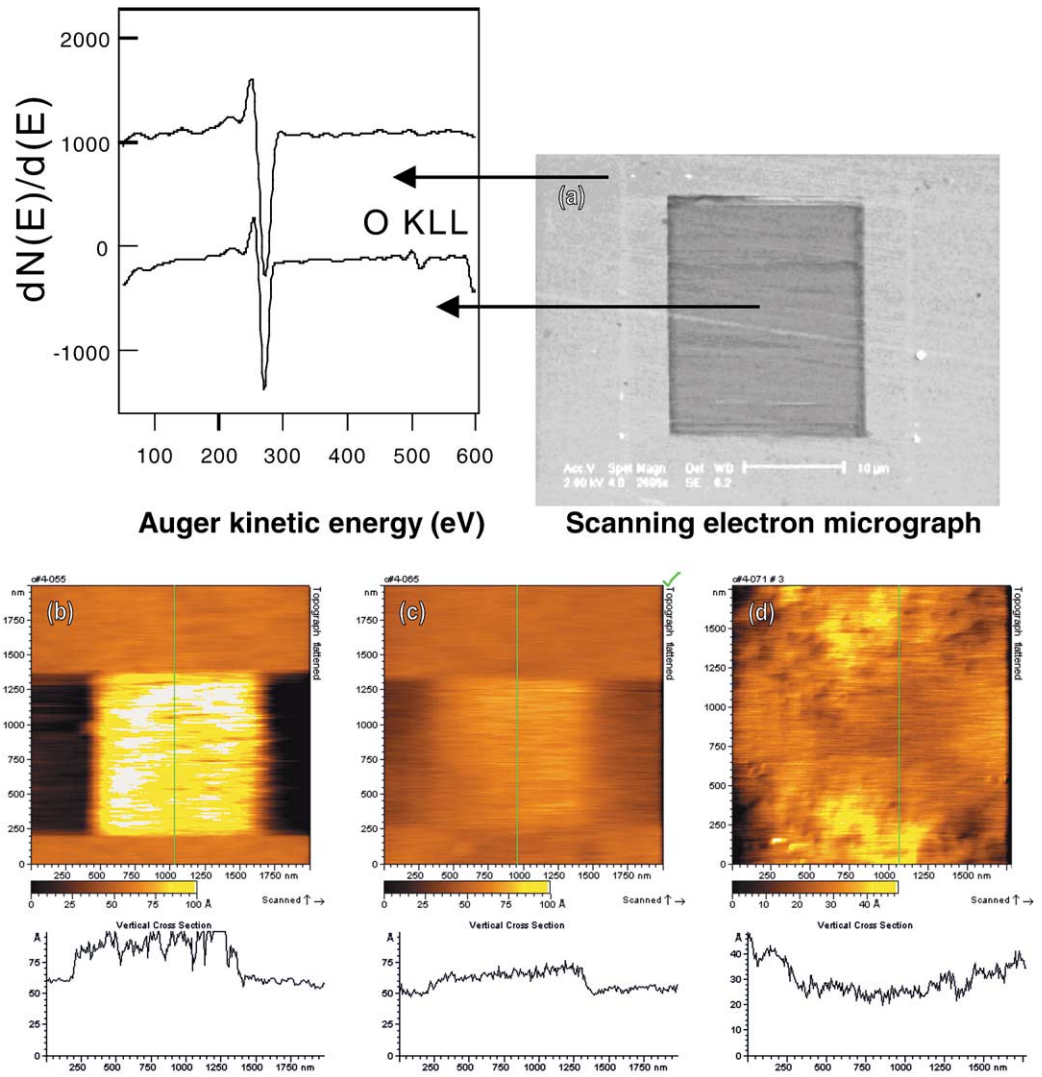

Fig. 7. (a) Scanning electron micrograph showing the lower secondary electron yield from the local anodic oxidized area (10×10 μm^2), and the corresponding scanning auger microprobe analysis which indicates that the modified area has a higher O KLL peak. (b–d) Local anodic oxidation with the diamond held at RT, 50 and 100 °C respectively, AFM performed in constant height mode.

fied area with an increase in substrate temperature. One effect of increasing the substrate temperature is to decrease the adsorption of moisture on the surface, if the adsorbed moisture acts as the electrolyte for the localized oxidation, the reduced contrast can be explained by the reduction in the coverage of moisture on the surface at higher temperature.

3.2. DOS of oxygenated diamond (100) surface from first principles theory

From both XPS and UPS data of the oxygenated diamond surfaces above, we can see a strong chemically shifted component and an increased in emission intensity near the Fermi level. To investigate the electronic structure of the oxygenated

diamond (1 0 0) surface, we applied the plane wave ab initio pseudopotential method within the LDF theory to calculate the surface and bulk DOS. Non-local norm-conserving pseudopotentials are created according to the prescription of Hamann et al. [25]. The Hedin–Lundqvist (HL) form of the exchange-correlation potential in the LDA [26] and a mixed basis representation are employed. The wave functions are expanded into plane waves up to a cutoff energy of 14.5 Ry. Considering the fairly sharp local orbital of C elements, we supplement the plane-wave basis with local orbital centered on the atomic sites, this is the so-called "mixed-basis technique" [27]. This technique was originally introduced by Louie et al. [28] to calculate the electronic structures of transition metals, and subsequently extended to include total energy and force calculations [29–32]. Usually just a few local orbital per atom are needed and when they are optimized carefully, most elements can be converged reasonably well with a plane wave cutoff of about 10 Ry.

Test calculations of bulk diamond have been done by ab initio pseudopotential with LDA (HL) to ensure the calculations are reliable for surfaces. The lattice constant obtained from current ab initio pseudopotential are 3.561 Å for diamond, which is in agreement with experimental data 3.567 Å. The bulk modulus of diamond is 479 GPa, within the range of experimental and calculated data [33]. We perform the DOS calculations for H:C(1 0 0) 2×1, O:C(1 0 0) 1×1 and bare C(1 0 0) 2×1 surfaces using the same program and cutoff energy. The slab geometries are employed to represent diamond surfaces. The bottom of the slabs is saturated by H. After performing the bulk calculations, we performed careful total energy calculations for the oxygenated diamond surface.

Two models of oxygen binding on the diamond (1 0 0) were used for calculating the DOS—the bridging (BR) oxygen model and the oxygen on-top (OT) model. The atomic models used for the calculation are shown in Fig. 8(a) and (b). In the BR model, the BR oxygen forms an ether-like linkage between the two carbon atoms in the $[\bar{1}\,1\,0]$ direction. In the OT model, the oxygen adopts a carbonyl-like binding mode on top of the carbon atom.

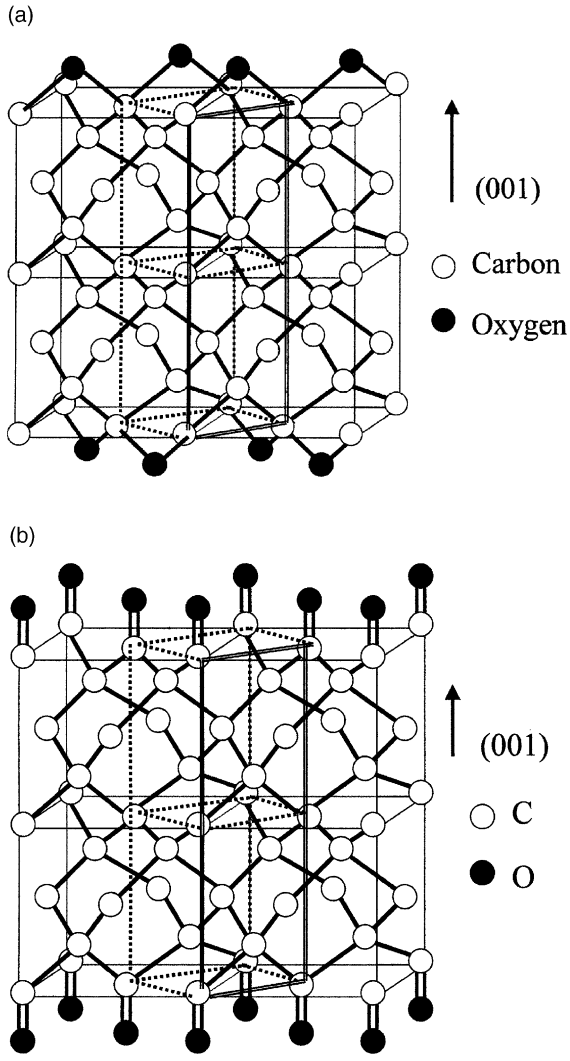

Fig. 8. (a) Atomic structural model of oxygenated diamond (1 0 0) adopting the "BR" model with the oxygen spanning the carbon atom in the [−1 1 0] direction and (b) atomic structural model of oxygenated diamond (1 0 0) adopting the "OT" model.

3.2.1. Relaxation of oxygenated C(100) surface

The slabs of oxygenated diamond (1 0 0) surface were fully relaxed by ab initio pseudopotential. The bond length of O—C was obtained as 1.51 Å for "BR" model (oxygen sites on bridge of carbons) and 1.26 Å for "OT" model (oxygen sites on top of carbons). These values agree quite well with previous calculations [18,34]. The multi-layer relaxation of oxygenated diamond (1 0 0) surface has

Table 1
Relaxation of O-diamond ($a_0 = 3.56$ Å) by ab initio pseudopotential

	Interlayer spacing (Å)				
	d_{12} (O–C1)	d_{23} (C1–C2)	d_{34} (C2–C3)	d_{45} (C3–C4)	d_{56} (C4–C5)[a]
BR					
Unrelaxed		0.8900	0.8900	0.8900	0.8900
Relaxed	0.8365	0.8789	0.8933	0.8913	0.8911
Δd (%)		−1.25	0.37	0.15	0.12
OT					
Unrelaxed		0.8900	0.8900	0.8900	0.8900
Relaxed	1.2595	0.8614	0.9002	0.8876	0.8904
Δd (%)		−3.21	1.15	−0.27	0.04

[a] Here, C5 is bulk-like layer, which is located in the center of the slab.

been determined. The results of the interlayer distances are listed in Table 1. The results suggest that the adsorbed O does not move along surface plane, but is relaxed along z-axis. From Table 1, one can see that the relaxation decreases from the surface into bulk. In the BR model, the interlayer distance between the first layer carbon and second layer carbon (C_1) is compressed while C_2, C_3, and C_4 are expanded. For the OT model, the interlayer spacing between the first and second layer carbon shows a greater contraction (3.7%) than that of the BR model while the interlayer spacing between second and third layer shows a corresponding expansion.

3.2.2. Layered-resolved DOS of oxygenated C(100)

The TDOS of H:C(1 0 0) 2 × 1, O:C(1 0 0) 1 × 1 (BR model and OT model) and bare C(1 0 0) 2 × 1 surfaces obtained by the above methods are plotted in Fig. 9. In the plot, we reference the binding energy scale to the valence band maximum (VBM). From the TDOS, it is clearly seen that there are no DOS states at the VBM for the H:C(1 0 0) 2 × 1 surface, in agreement with previous photoemission studies and theoretical calculations [35,36]. Strong DOS states can be observed at the VBM for the O:C(1 0 0) 1 × 1 (BR model) and the bare C(1 0 0) 2 × 1. These first principles results obtained are in good agreement with our photoemission spectra which show an increase in emission intensity near the VBM after the adsorption of O, as well as after the generation of a bare 2 × 1 surface. To reveal the origin of the occupied states below the VBM as well as unoccupied states in the band gap, we plot the layer-resolved partial density of states (LDOS) for the two types of oxygenated diamond surfaces, shown in Figs. 10–15. Only the LDOS of adatom (O), top-most carbon layer (C_1) and slab-center carbon layer (bulk-like, C_{1-5}) are plotted for comparison.

LDOS of the first, second, third and fifth carbon layers for diamond adopting the bridged oxygen configuration (BR model) are shown in Fig. 10. The LDOS shows the presence of occupied surface and empty surface states in the gap of the near surface layers. The LDOS of the first two layers show DOS intensity near the VBM whereas the bulk diamond layers (third and fifth layers) have a weaker DOS intensity at the VBM. A strong oxygen-induced state deep in the valence band at −22 eV which extends beyond the first layer to the second layer carbon can be seen. This state can be observed experimentally in the X-ray induced valence band spectrum of oxygenated diamond (Fig. 16(d)), as the technique has a higher cross-section for the O 2s state. To correlate the origin of the features in the LDOS of carbon, we look at the DOS of the oxygen adlayer in Fig. 11 and the s and p-resolved DOS of the first layer carbon that is bonded to the oxygen in Fig. 12. The strong state observed at −22 eV in Fig. 10, which manifests in both the C 2s and $2p_z$ orbitals (sp_z hybrid orbital), is induced by O 2s, as can be judged by the strong O 2s feature in Fig. 11 at −22 eV. Strong surface state emission at the VBM (0 to −2 eV) in this case originates mainly from the non-bonded O lone pairs because no such counterpart

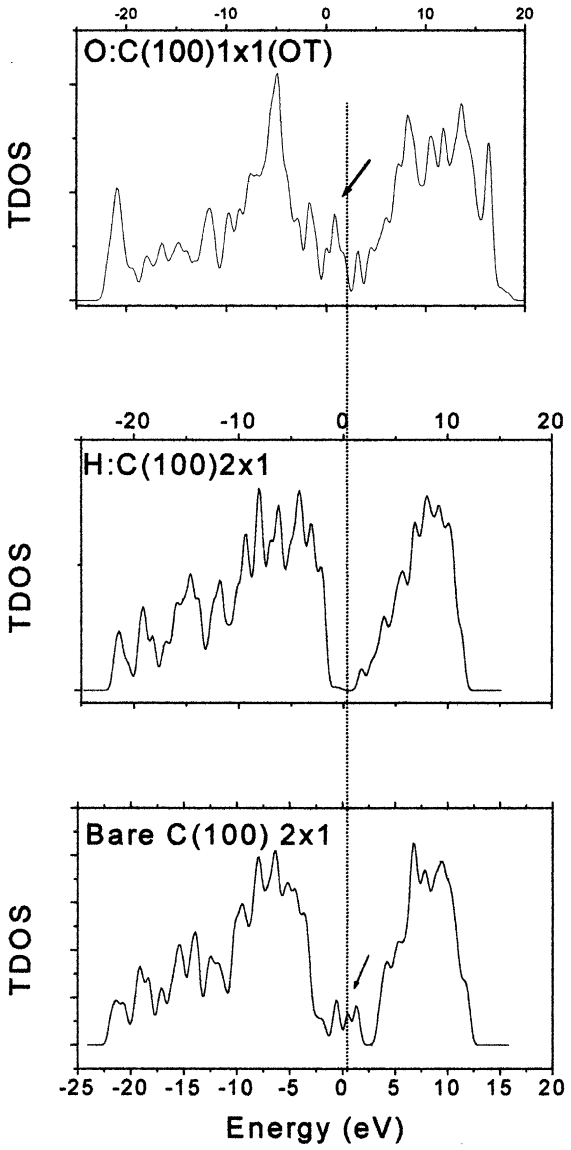

Fig. 9. The TDOS of diamond surfaces. From top to bottom are O:C(1 0 0) 1×1 (OT model), H:C(1 0 0) 2×1 and bare C(1 0 0) 2×1 surfaces. Surface states in the band gap of O:C(1 0 0) 1×1 surface and bare C(1 0 0) 2×1 surface can be observed.

state is seen in the LDOS of the carbon. DOS states at -4 to 5 and -8 eV have contributions from the O 2p and C 2p bonding orbitals, in other words, these states may be interpreted in terms of CO-like molecular orbitals.

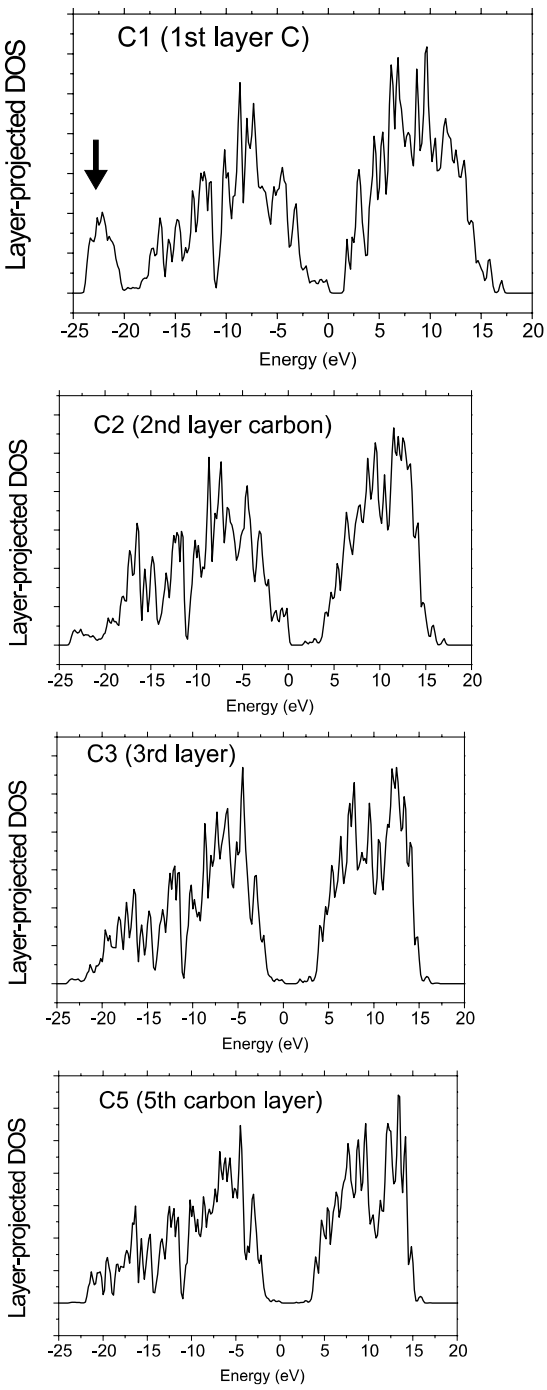

Fig. 10. Layer-projected DOS of carbon in different layers from surface into bulk (C1 → C2 → C3 → C5) of O:C(1 0 0) 1×1 adopting the BR model.

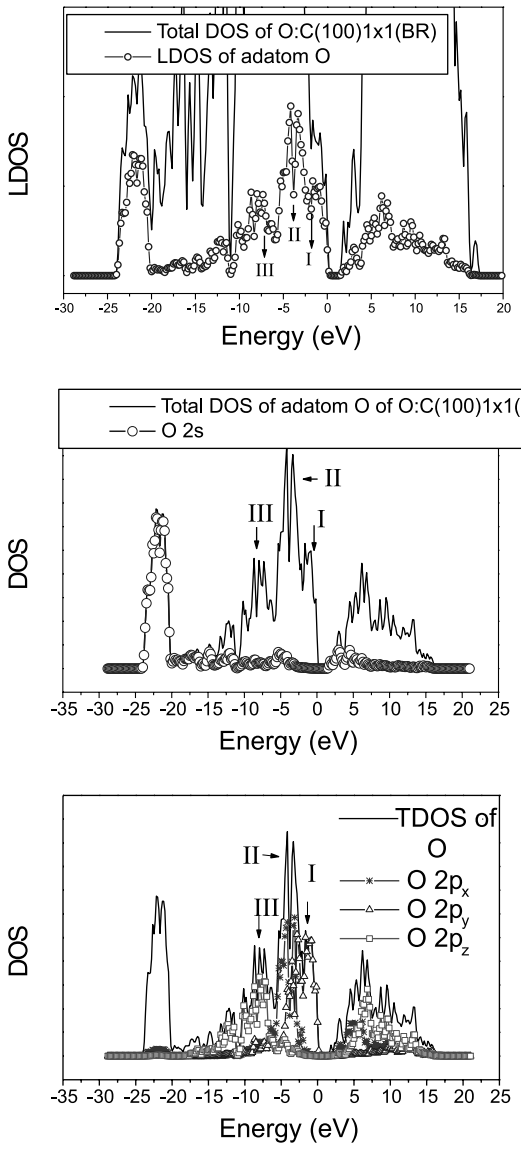

Fig. 11. Contribution of adatom O to the TDOS of O:C(1 0 0) 1×1 adopting the BR model (a) open circle: LDOS of adatom O; solid line: TDOS (b) open circle: O 2s contribution to LDOS of adatom O; solid line: LDOS of adatom O; (c) circles: O 2p contribution to LDOS of adatom O; solid line : LDOS of adatom O.

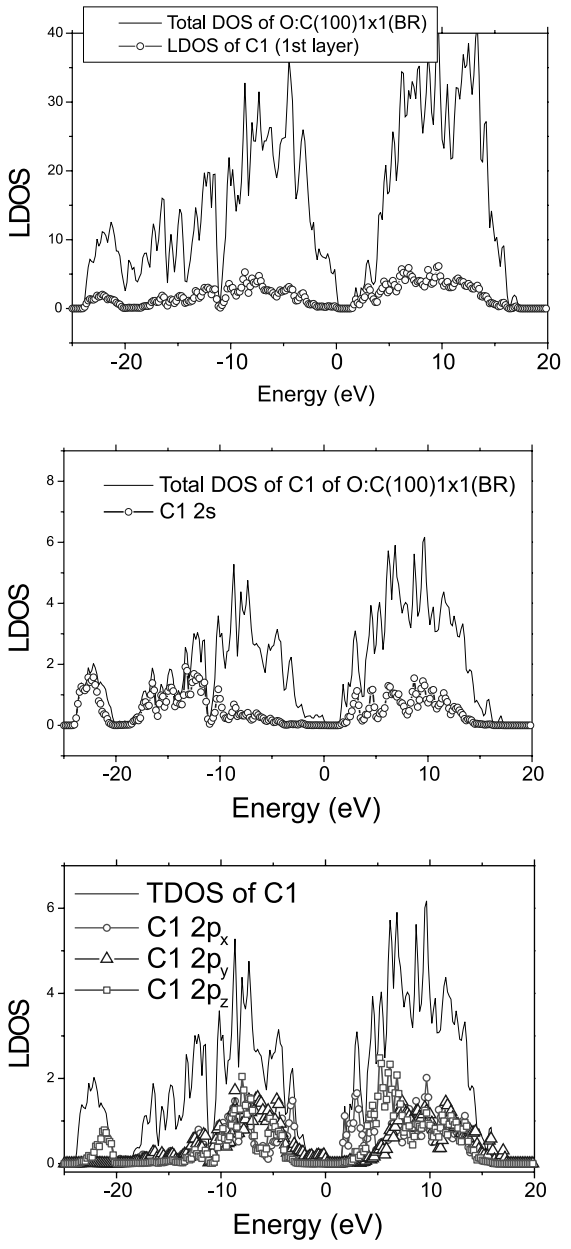

Fig. 12. Contribution of first layer carbon (C_1) to the TDOS of O:C(1 0 0) 1×1 adopting the BR model (a) open circle: LDOS of C_1; solid line: TDOS, (b) open circle: C 2s contribution to LDOS of C_1; solid line: LDOS of C_1 and (c) circles: C 2p contribution to LDOS of C_1; solid line: LDOS of C_1.

Fig. 13 shows the LDOS of C for oxygenated diamond adopting the oxygen OT model. A prominent peak at -5 eV below VBM, along with a band of states in the band gap can be seen. The -5 eV peak has contribution from hybrid O 2s, O $2p_x$ as well as C $2p_x$ orbitals, as can be judged from the O and C s and p-resolved LDOS in Figs. 14 and 15 respectively, so this is a CO-like molecular

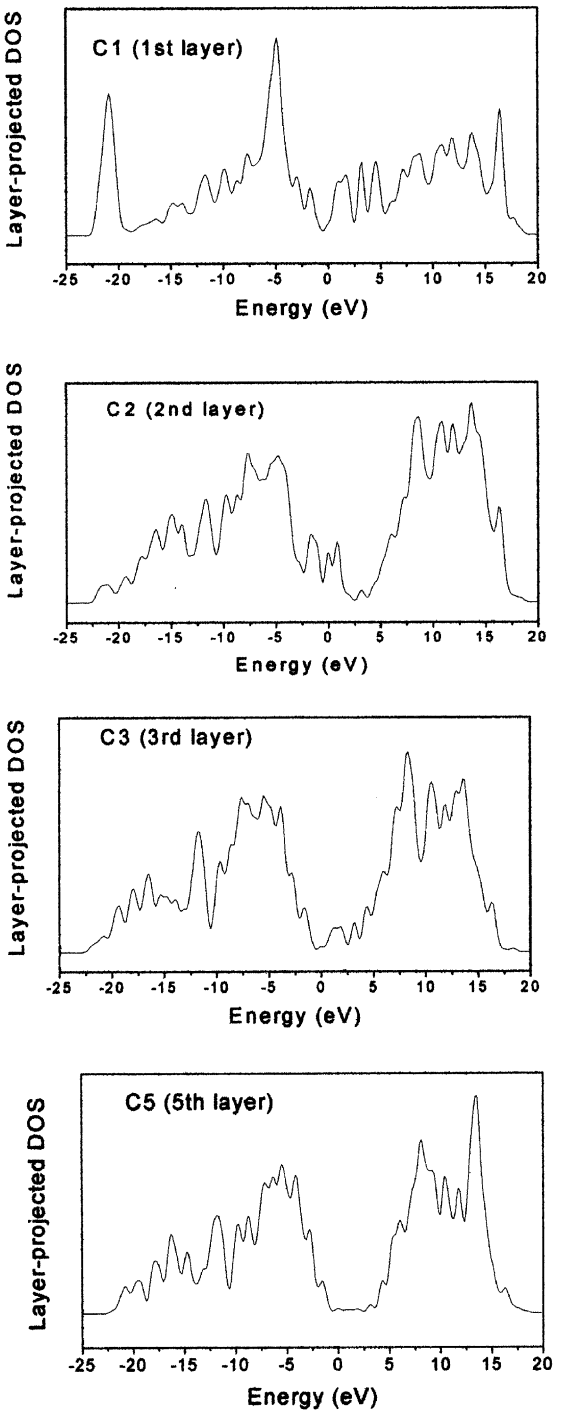

Fig. 13. LDOS of carbon in different layers from surface into bulk (C1 → C2 → C3 → C5) of O:C(1 0 0) 1 × 1 adopting the OT model.

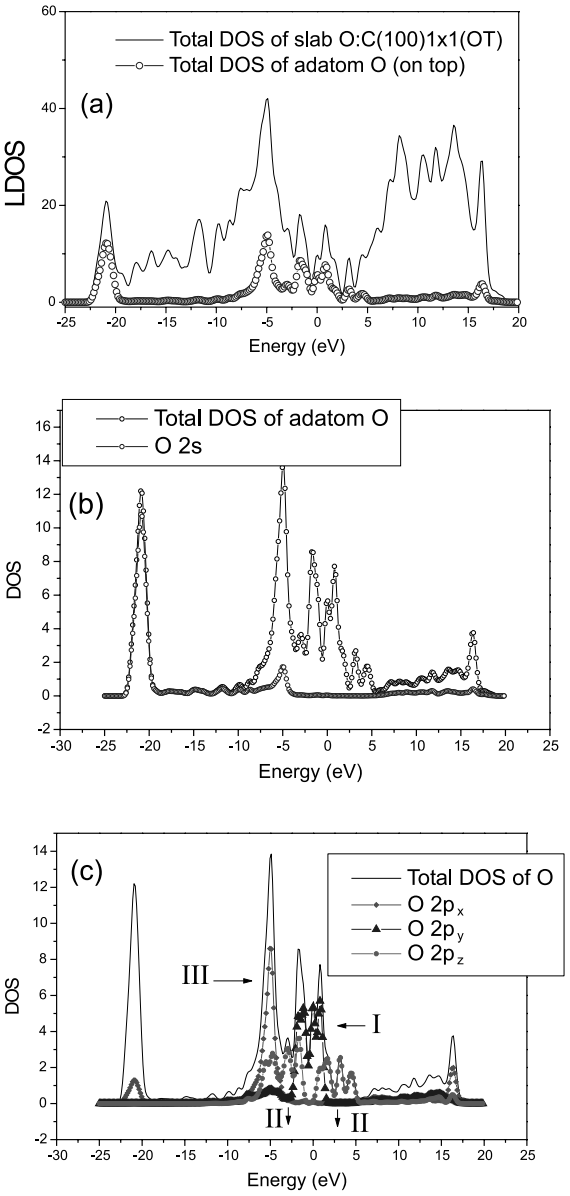

Fig. 14. Contribution of adatom O to the TDOS of O:C(1 0 0) 1 × 1 adopting the OT model (a) open circle: LDOS of adatom O; solid line: TDOS, (b) open circle: O2s contribution to LDOS of adatom O; solid line: LDOS of adatom O and (c) circle: O 2p contribution to LDOS of adatom O; solid line : LDOS of adatom O.

orbital. The effect of oxygen adopting the OT model is the closing of the surface band gap due to an almost continuous band of states in the gap.

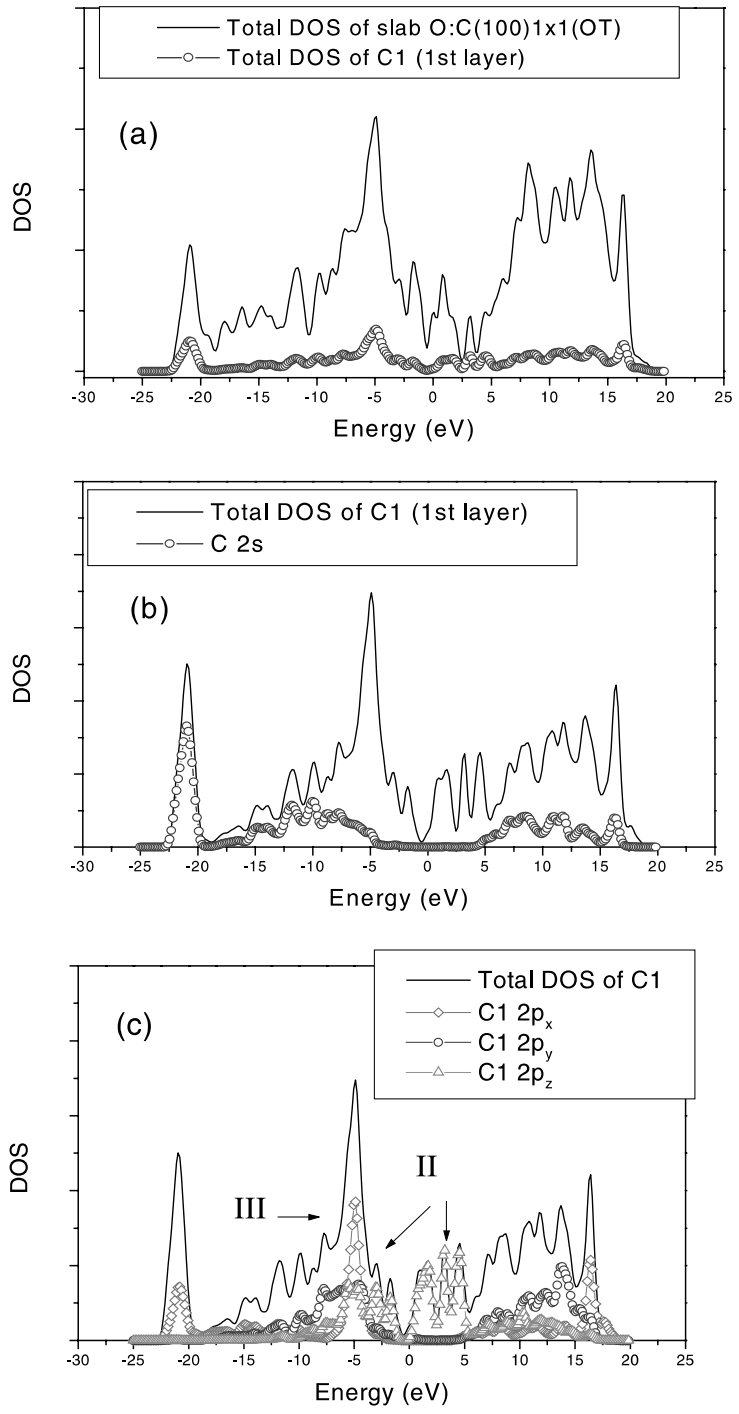

Fig. 15. Contribution of first layer carbon (C_1) to the TDOS of O:C(1 0 0) 1×1 adopting the OT model (a) open circle: LDOS of C_1; solid line: TDOS, (b) open circle: C 2s contribution to LDOS of C_1; solid line: LDOS of C_1 and (c) circles: C 2p contribution to LDOS of C_1; solid line: LDOS of C_1.

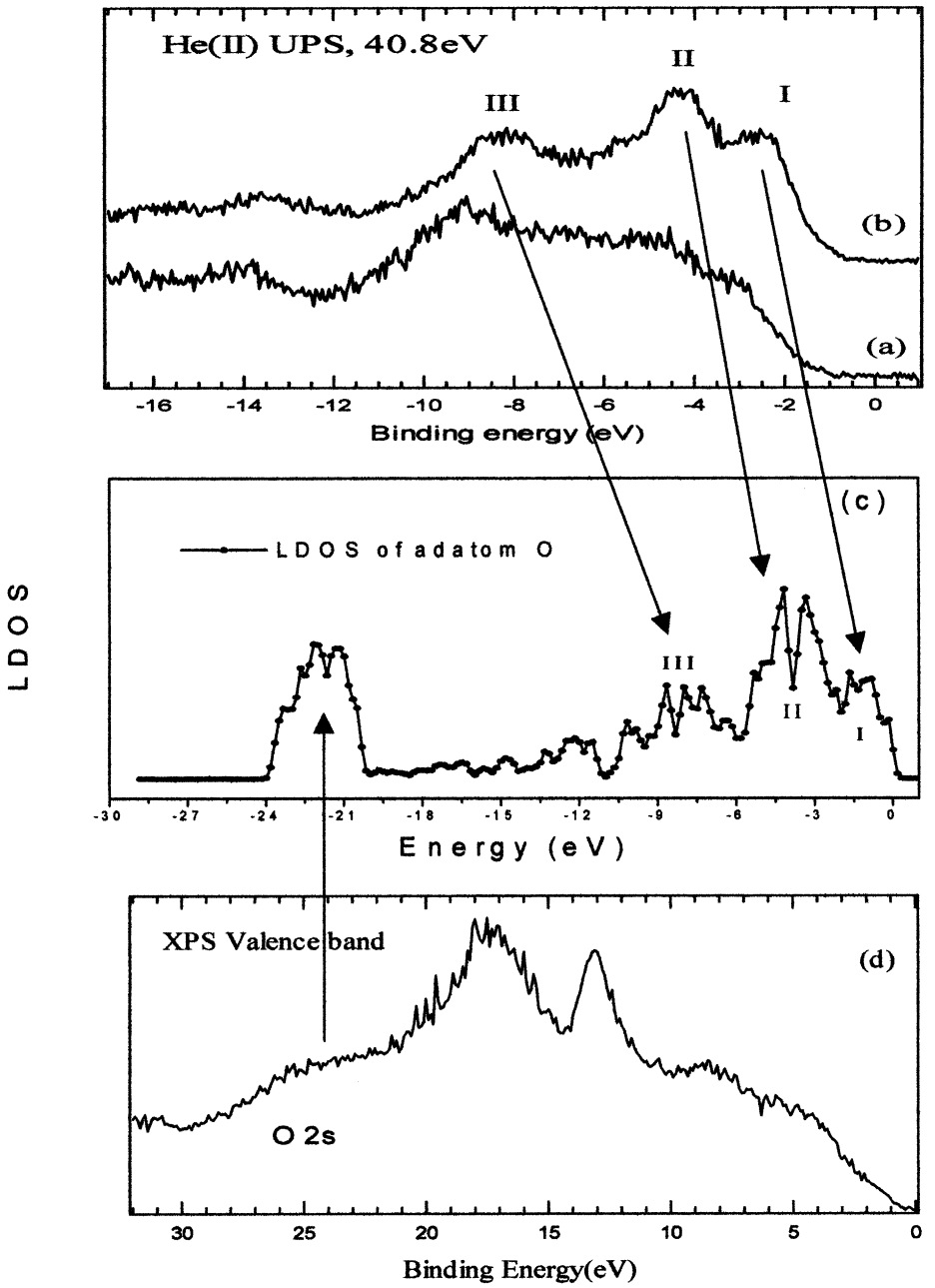

Fig. 16. UPS He(II) spectum of C(1 0 0) with (a) 0.1 ML O coverage; (b) 1 ML O coverage; (c) LDOS of adlayer O adopting the BR model and (d) XPS valence band structure of C(1 0 0) with 1 ML O coverage.

The charge transfer effect of CO-like orbital is strong enough to permeate to the third carbon layer, this can be judged from the closing of the surface band gap of the second as well the third carbon layers, shown in the LDOS of Fig. 13. The OT model is distinguished by the presence of pπ bonding orbitals between carbon and oxygen atoms as well as the close proximity of two oxygen

lone pairs on one carbon atom. Very prominent occupied and unoccupied surface states can be seen as a result in the LDOS of O and first layer carbon in Figs. 14 and 15. Occupied state due to sp-hybridized carbon orbital and O 2s can be seen at −22 eV. This is the solid phase equivalent of the 4σ molecular orbital of gaseous CO. Strong O-induced surface states can be seen between 0 and 5 eV in Fig. 14. Peak I, situated in the middle of the energy gap, is assignable to non-bonded oxygen lone pairs because it has no counterpart in the LDOS of carbon. Peak II, with its DOS spanning between −5 and 5 eV, is observable in the LDOS of O $2p_z$ (Fig. 14(c)) as well as C $2p_z$ (Fig. 15(c)) and has its DOS split into two halves between the VBM in the respective LDOS of each. Therefore, peak II is attributable to the bonding and anti-bonding π states arising from pπ overlap between the C 2p and O 2p in the C═O bond.

A comparison of our calculated DOS with the experimentally observed valence band spectra recorded using He(II) (40.6 eV) and X-ray excitation is shown in Fig. 16. Fig. 16(a) shows the spectrum of the C(1 0 0) surface covered with only 0.1 ML O following O-atom beam treatment at room temperature, whilst Fig. 16(b) shows similar treatment at 300 °C, where a coverage of close to 1 ML O is attained. The spectral profile of the oxygenated diamond is distinguished by an *increase* in the emission intensity of three states at −2 eV (labeled "I"), −4 eV (labeled "II") and −8 eV (labeled "III") in the He(II) valence band spectrum, and the growth of a peak between −20 and −25 eV in the X-ray valence band, labeled as "O 2s", shown in Fig. 16(d). The LDOS of O adlayer for the BR model is shown in Fig. 16(c) for comparison. The calculated DOS displays four peaks at −2, −4, −8 and −22 eV which are similar in positions to the experimentally observed ones, and which are attributable to the non-bonded lone pair (O $2p_y$), bonded O $2p_x$ and O $2p_y$ states respectively. The peak at −22 eV attributable to O 2s can be observed in the X-ray excited valence band spectrum in Fig. 16(d).

Comparing the calculated DOS of the BR model with the OT model reveals that peak III (5 eV) in the OT model is a hybrid between O 2s and O 2p, whereas it is exclusively O 2p in the BR model. The BR model shows a peak at −8 eV (peak III) assignable to bonding O $2p_z$, but this state is absent in the OT model because the O $2p_z$ of the OT model is shifted up in energy to −5 eV due to involvement in the pπ bonding. Both calculated models predict strong emission intensity near the VBM because of electron density of the non-bonded oxygen lone pair. It is difficult to distinguish by laboratory UPS alone whether the BR model is favored over the OT model since a coexistence of both binding modes may be present in practice. The relatively longer mean free path of 40 eV electrons used in laboratory UPS means that the surface oxygen DOS contribution is only a small fraction of the total bulk diamond DOS sampled. Future experiments using synchrotron photoemission facilities may be able to resolve the different binding modes.

4. Discussion

The experiments show that the oxygenation of diamond must proceed under controlled conditions to prevent etching and roughening of the diamond surfaces. At low oxidation temperature (below 300 °C), only partial coverage of the hydrogenated surface with oxygen could be achieved, as verified by both ERDA and TOF-SIMS. This observation is supported by the HREELS and Auger studies of Pehrsson and Mercer [1,2] which reported that oxidation proceeded in two stages on heated diamond sample. The actual mechanism is complex and involves multiple site and coverage dependent factors. Pehrsson reported that only about 1/4 ML was attained during the initial stages of oxidation at RT. At elevated temperatures, a higher coverage could be achieved and there is an upward shift in the wave number of ν(C═O) peak because of a change in ketones-dominated oxidation states to higher oxidation states such as lactones, carboxylic acids and carboxylic anhydrides [1,2].

We have applied ERDA and TOF-SIMS to quantify the absolute surface D content after exposure to an atomic O. The low thermal energy of oxygen atoms generated by our source possibly account for the inefficient O─D exchange at RT. It must be borne in mind that in high-pressure

plasma CVD system, the situation could be different due to the presence of energetic species such as O_2^+ and O^+. The restricted uptake of O at low temperature may be due to the adsorption of O only on sites such as facets and step edges that are rich in reactive, unpaired electrons. When the substrate temperature was increased to 300 °C during the O atomic beam treatment, at least 90% replacement of the surface D by O could be achieved. This suggests that the gas-phase O and surface D exchange mechanism proceeds via thermally activated mechanism. The first step could involve the insertion of O into C—D bonds to form C—OD or C=O, these steps will likely have an activation barrier so a thermal activation may assist the insertion process. Both RHEED and AFM reveal that the surface remains relatively smooth at the oxidation temperature of 300 °C, in contrast to rapid etching and roughening of the surface at elevated temperatures. The roughening is a result of CO and CO_2 desorption from the surface which proceeds at temperatures >500 °C [5]. Therefore a treatment temperature of 300 °C could be concluded to be most suitable for the oxygenation of the diamond surface by atomic O, since the surface chemistry was restricted to surface exchange of D by O, and did not extend to etching of the diamond matrix by O to form gaseous CO and CO_2. The oxygenated diamond surface also represents a more efficient temperate than the hydrogenated surface for generating a clean diamond surface because a clean 2×1 surface could be attained at 800 °C following the desorption of CO and CO_2 from the surface, and this process occurs at temperatures about 200 °C lower than that required for H desorption from the hydrogenated surface.

The 1×1 surface structure observed on the oxygenated diamond (1 0 0) can arise from either BR or OT oxygen atoms, we are not able to distinguish between the two possibilities here although HREELS studies by Pehrsson suggest the possibility of a mixed configuration [1,2]. Our XPS study indicates the occurrence of multiple oxidation states on the surface, with the growth of higher oxidation states becoming more pronounced at higher oxidation temperature. Chemically shifted component at ~1–2 eV from the bulk peak is attributable to C=O or C—O species, and there are the main oxidation state below 400 °C. At higher oxidation temperatures, higher oxidation states due to carboxylic or anhydride species which are chemically shifted by 3.2 eV from the bulk C 1s peak are observed to grow. The appearance of these higher oxidation state feature is accompanied by a roughening of the diamond surface, so a different oxidation mechanism may be operational on defects and facets in this instance [2].

Semi-empirical cluster simulation showed that half or full monolayers O atoms added to the OT sites could yield a 1×1 arrangement with no surface reconstruction [34]. A 0.5 ML of oxygen added to the bridge site on dimerized surface cleaved the C—C dimers and an unreconstructed 1×1 arrangement could result. We observed that the exchange of chemisorbed D by atomic O was relatively inefficient at RT, so a weak 2×1 pattern persists. A clear 1×1 pattern only emerges when the surface coverage of D reduces by more than 50%. If the substrate temperature was held at 500 °C during the O-plasma treatment, irreversible, rapid roughening of the diamond sample resulted. When a spotty 1×1 RHEED pattern was obtained, the 2×1 pattern could no longer be recovered even after heating to 1200 °C, suggesting that surface roughness sustained during high-temperature oxidation treatment inhibited reconstruction. The background pressures of O employed in this work was in the 1×10^{-3} Torr range, this is equivalent to a concentration of about ~1000 ppm range in typical CVD conditions. This provides an insight into the origin of the O suppression of diamond growth when its concentration exceeds a certain threshold in the CVD gas feed. At the typical temperature used for diamond CVD (700–800 °C), a high O concentration will lead to extensive etching of the diamond and prevent diamond deposition. Our ERDA and TOF-SIMS studies also suggest that the temperature range of 300–500 °C is suitable for the low temperature growth by O addition into the conventional H_2–CH_4 gas feed since the exchange of surface H by the atomic O can proceed efficiently at this temperature, thus activating the surface sites and creating dangling bonds for reaction with hydrocarbon precursors during diamond CVD.

Ultra-shallow depth profiling by TOF-SIMS discovered no evidence of surface incorporation of D or O within 10 nm of the surface following RF-D or O plasma loading at 800 °C. The depth profiles presented here were obtained by sputtering a large area (300–500 μm^2) with a pulsed Ar^+ sputter beam (1 keV, 16 nA, 10^7 ions/pulse). The sputtering rate could be tuned as low as 1 ML per tens of seconds, achieving ultra-shallow depth profiling. The rapid decay of the D^- signal to the background level within the shallow information depth indicated that the D adsorption was restricted to a surface monolayer only and that there was no diffusion of D into the bulk. Previous SIMS reported the diffusion of H in the subsurface region (20 nm below surface) [37]. It is possible that the origins of the detected H originate from H trapped in the growing layers during the CVD process instead of post-hydrogen plasma treatment. A recent ERDA measurement of H in type IIa single crystal diamond also found no evidence of the presence of H in bulk and subsurface region due to plasma loading [37]. Therefore models which explain the high surface conductivity of hydrogenated diamond layer after H-plasma treatment by invoking the mechanism of incorporated H in the subsurface region [38] are not supported by our results. The confinement of both D and O adlayer to the surface regions means that what we are sampling by ERDA and TOF-SIMS is a direct mapping of the aerial densities on the surface following O—D exchange. The result indicates that atomic O could induce desorption of the chemisorbed D at RT. We also found evidence of the existence of OD species on the surface following low-temperature O atom beam treatment. At 300 °C or higher, a near complete exchange of chemisorbed D by atomic O occurred to attain saturation O density on the surface.

Local anodic oxidation of the C(1 0 0) surface in ambient conditions is shown to be a feasible way of creating oxygenated domains on hydrogenated samples. The oxidation mechanism is different to that of dry oxidation with an atomic beam source, one of the differences being that the oxidation efficiency decreases with substrate temperature in the local anodic method. In principle, the resolution of AFM allows nanometer-scale feature to be created so this technique is promising for nanotechnology applications which can exploit differentially oxidized and hydrogenated areas [9]. The ability to impose a graded potential during the line scanning also allows the creation of oxygenated regions with a gradient in oxygen concentration, as we have demonstrated in Fig. 6. In practice however, the difference in contrast following the line scanning, whether by lateral force or normal force imaging, is observable only if the diamond surface has an initial surface corrugation less than 5 nm. The local anodic oxidation mechanism involves moisture in the air acting as an electrolyte for the oxidation. We have demonstrated that increasing the substrate temperature reduces the moisture retention on the surface and decreases the oxidation efficiency. We have tried reversing the polarity on the AFM tip and introduced hydrogen on the surface during the process to see if the process was reversible, that is replacing the chemisorbed oxygen with hydrogen, but obtained negative results. Therefore the oxygenated domains are very stable. This result suggests that electrochemical oxidation may be the most effective way of oxidizing the diamond surface at low temperature. This technique may provide a way of creating spatially resolved domains with differing hydrophilicities on the diamond surface. Recently it has been shown that the oxidized diamond template as a good support for nickel catalyst in the methane synthesis reaction [44]. Creating spatially resolved, nano-scale C—O terminated sites on diamond may therefore create preferential binding site for polymers or nano-metals where the diamond template may provide advantages in terms of air stability and oxidation resistance.

Klauser performed valence band spectroscopy on oxygenated C(1 1 1) and observed oxygen-induced emission band at 4.2 and 8 eV [4]. They suggested that the 8 eV peak was related to O 2p whilst the 4.2 eV peak might be related to CO-like molecular orbitals. The 4.2 eV peak however was not conspicuous in their valence band spectra for the 0.5 ML O-dosed surface and was deduced from a difference spectra between annealed surface and oxygen-dosed surface. In this work, we directly observed prominent emission states at 3 and 5 eV in the He (II) spectra, and enhanced intensity

centered at 3.5 eV in the He (I) spectra for the oxygenated diamond. One reason for the stronger intensity in our study could be related to the higher O coverage (~1 ML) which was attained following O atom beam treatment at 300 °C. The UPS spectrum of C(1 0 0) irradiated with O atom beam at RT is very similar to that observed by Klauser, only a weak gain in emission intensity near 4 eV was detected. From the LDOS calculation, we are able to assign the experimentally observed oxygen-induced surface states at ~4–5 eV as well as 8 eV to CO-like molecular orbitals because corresponding features in the C 2p LDOS can be seen. The gas-phase CO molecule has photoionization potentials from the 5σ, 1π and 4σ molecular orbitals at around 14, 17 and 20 eV [39]. For the CO/Ni(1 0 0) surface for example, the overlapping 5σ and 1π levels were observed at 8 eV and the 4σ level at 11 eV, relative to the Fermi level. Adsorption on C(1 0 0) in this study was found to shift the energies of these CO-like molecular orbitals to ~4 and ~8 eV, where relative differences in the DOS intensity exist depending on the binding mode of O adopted (OT or BR model).

Dramatic changes in the electronic properties of the surface occur with oxygen adsorption. Oxygen bonding creates inhomogeneous electronic surroundings of the surface carbon atom because of the presence of oxygen and carbon bonding pair, non-bonding oxygen lone pairs and antibonding dipoles. These strongly localized features will be markedly different between oxygen adopting different binding modes. Due to charge transfer from carbon to oxygen in the oxygen bond formation, the energy band of the host material is modified. These modifications are stronger in the case of the oxygen adopting the OT configuration. Calculations of multi-layer relaxation shows that the interlayer distance between the first and second layer carbon is contracted severely in the OT model. Strong oxygen induced features can be observed in the LDOS up to the third carbon layer, suggesting strong charge transfer in the OT model. Evidence for charge transfer arises from the shift of the C 1s core level peak to increasingly higher binding energy with the uptake of oxygen on the surface, as shown in the XPS study in Fig. 2, which is characteristic of downward band bending. It has been suggested by Shirafuji [40] as well as Gonon [41] that on an oxygen-terminated surface produced by oxygen-plasma treatment, the surface energy band bends downwards to give a depletion layer for holes because of the presence of donor-type surface states existing at about 1.7 eV above the valence band maximum. In both oxygen binding models, our ab initio calculations show that the presence of oxygen lone pairs introduce occupied surface states near the VBM. These donor type surface states induced by oxygen adsorption may be responsible for surface Fermi level pinning observed by Kiyota for Schottky-barrier formation on oxygenated diamond [42]. An aerial density of O on the surface in the range of 10^{15} cm^{-2} is several order of magnitude higher than the theoretical value of $2–4 \times 10^{12}$ cm^{-2} required for pinning the surface Fermi level [43]. Alternatively, the higher density of defects on oxidized diamond surface can also contribute to the Fermi level pinning.

Another influence of oxygen adsorption is the conversion of the NEA condition on diamond into a PEA condition. It is apparent from the DOS calculation that the surface termination by oxygen closes the surface band gap. We can see for example that the termination of C(1 0 0) by C=O (OT model) introduces π antibonding states as well as non-bonding lone pair states into the gap. The narrowing of the surface gap will place the vacuum level within these states, even though the bulk CBM can be higher than the vacuum level. Assuming that the presence of these oxygen-induced gap states now places the vacuum level within these gap states, it means that secondary electrons generated in the photoemission process will quasi-thermalized to these oxygen-induced gap states and be trapped near the surface rather than spontaneously escape into the vacuum, which it may do in the absence of these gap states. The irreversibility of the positive electron affinity observed in this study following the desorption of oxygen from the surface provides evidence for active exchange of the surface D by atomic O, in contrast to the situation where the O is simply co-adsorbing with the D.

5. Conclusion

Both macroscopic and microscopic oxidation of the diamond (1 0 0) surface has been investigated. Atomic O beam treatment of C(1 0 0) at 300 °C is effective for the surface exchange of chemisorbed D by O. High-temperature atomic O treatment leads to the rapid roughening of the diamond surface and the production of high oxidation states on the surface. The desorption of O from the diamond surface at 800 °C results in the appearance a 2×1 surface state due to the clean surface π-bond reconstruction. We have verified that the micron-sized area prepared by local anodic oxidation on hydrogenated diamond using AFM writing is oxygen rich. The changes in valence band spectral features of diamond (1 0 0) following exposure to atomic O beam have been studied. The adsorption of O results in the emergence of several oxygen-induced surface state features in the valence band spectra. Experimentally observed oxygen-induced surface states at ~4–5 eV as well as 8 eV can be assigned to CO-like molecular orbitals as confirmed by the correlated peaks in both the LDOS of the oxygen adlayer and substrate carbon. Non-bonded oxygen lone pair contributes strongly to states at the VBM for surface oxygen adopting the OT configuration as well as the BR configuration. The OT configuration has a greater degree of contraction in the interlayer spacing of the near surface carbon layers as well as a higher degree of charge transfer from the bulk to the oxygen compared to the BR configuration. Compared to the BR model, the OT model is distinguished by strong bonding and antibonding π states arising from pπ overlap between the C 2p and O 2p in the C═O bond which narrows the surface band gap.

Acknowledgements

This project is funded by NUS academic research grant number R-143-000-061-112 entitled "Growth and etching of wide band gap semiconductors".

References

[1] P.E. Pehrsson, T.W. Mercer, Surf. Sci. 460 (2000) 49.
[2] P.E. Pehrsson, T.W. Mercer, Surf. Sci. 460 (2000) 74.
[3] M.Z. Hossain, T. Kubo, T. Agura, N. Takagi, T. Tsuno, N. Fujimori, M. Nishijima, Surf. Sci. 436 (1999) 63.
[4] R. Klauser, J. Chen, T. Chuang, L. Chen, M. Shih, J. Lin, Surf. Sci. 356 (1996) L410.
[5] R.E. Thomas, R.A. Rudder, R.J. Markunas, J. Vac. Sci. Technol. A 10 (1992) 2451.
[6] H. Tamura, K. Sugisako, Y. Yokoi, S. Takami, M. Kubo, K. Teraishi, A. Miyamoto, Phys. Rev. B. 61 (2000) 11025.
[7] B.L. Mackey, J.N. Russel Jr., J.E. Crowell, P.E. Pehrsson, B.D. Thomas, J.E. Butler, J. Phys. Chem. B 105 (2001) 3803.
[8] C. Bandis, B.B. Pate, Phys. Rev. B 52 (1995) 12056.
[9] M. Tachiki, T. Fukuda, K. Sugata, H. Seo, H. Umezawa, H. Kawarada, Appl. Surf. Sci. 159–160 (2000) 578.
[10] P. Gluche, A. Aleksor, A. Vescan, W. Eberl, E. Kohn, IEEE Electron. Dev. Lett. 18 (1997) 547.
[11] J.S. Foord, L.C. Hian, R.B. Jackman, Diamond Relat. Mater. 10 (2001) 701.
[12] M. Yoshimoto, M. Furusawa, N. Nakajima, M. Takakura, Y. Hishitani, Diamond Relat. Mater. 10 (2001) 295.
[13] T. Ando, K. Yamamoto, M. Ishii, M. Kamo, Y. Sato Jr., Chem. Soc. Farad. Trans. 89 (1993) 3635.
[14] J.C. Zheng, X.N. Xie, A.T.S. Wee, K.P. Loh, Diamond Relat. Mater. 10 (2001) 500.
[15] X.M. Zheng, P.V. Smith, Surf. Sci. 262 (1992) 219.
[16] T. Frauenheim, U. Stephan, P. Blaudeck, D. Porezag, H.G. Bussmann, W. Zimmermann-Edling, S. Lauer, Phys. Rev. B 48 (1993) 18189.
[17] B.N. Davidson, W.E. Pickett, Phys. Rev. B 49 (1994) 5662.
[18] S.H. Yang, D.A. Drabold, J.B. Adams, Phys. Rev. B 48 (1993) 5261.
[19] J. Furthmüller, J. Hafner, G. Kresse, Phys. Rev. B 53 (1996) 7334.
[20] H. Kawarada, H. Sasaki, A. Sato, Phys. Rev. B 52 (1995) 11351.
[21] S. Pettrick, C. Benndorf, Diamond Relat. Mater. 10 (2001) 519.
[22] H. Yagi, A. Hatta, T. Ito, Appl. Surf. Sci. 137 (1999) 50.
[23] A. Benninghoven, F.G. Rüdenauer, H.W. Werner, Secondary Ion Mass Spectrometry, Basic Concepts, Instrumental Aspects, Application and Trends, John Wiley, New York, 1987.
[24] E.S. Snow, G.G. Jernigan, P.M. Campbell, Appl. Phys. Lett. 76 (2000) 1782.
[25] D.R. Hamann, M. Schluter, C. Chaing, Phys. Rev. Lett. 43 (1979) 14941.
[26] L. Hedin, B.I. Lundqvist, J. Phys. C 4 (1971) 2064.
[27] C.T. Chan, K.M. Ho, in: J.R. Chelikowsky, S.G. Louie (Eds.), Quantum Theory of Real materials, Kluwer Academic, Boston, 1996.
[28] S.G. Louie, K.M. Ho, M.L. Cohen, Phys. Rev. B 19 (1979) 1774.

[29] C.L. Fu, K.M. Ho, Phys. Rev. B 28 (1983) 5480.
[30] K.M. Jo, C.L. Fu, B.N. Harmon, Phys. Rev. B 28 (1983) 6687.
[31] C. Elsasser, N. Takeuchi, K.M. Ho, C.T. Chan, P. Braun, M. Fahnle, J. Phys.: Condens. Mater. 2 (1990) 4371.
[32] K.M. Ho, C. Elsasser, C.T. Chan, M. Fahnle, J. Phys.: Condens. Mater. 4 (1992) 5189.
[33] J.-C. Zheng, C.H.A. Huan, A.T.S. Wee, R.-Z. Wang, Y.-M. Zheng, J. Phys. Condens. Matter. 11 (3) (1999) 927, and references therein.
[34] S. Skokov, B. Weiner, M. Frenklach, Phys. Rev. B 49 (1994) 11374.
[35] T. Frauenheim, U. Stephan, P. Blaudeck, D. Porezag, H.G. Bussmann, W. Zimmermann-Edling, S. Lauer, Phys. Rev. B 48 (1993) 18189.
[36] G. Francz, P. Oelhafen, Surf. Sci. 329 (1995) 193.
[37] K. Hayashi, S. Yamanaka, H. Watanabe, T. Sekiguchi, H. Okushi, K. Kajimura, J. Appl. Phys. 81 (1997) 744.
[38] I.Z. Machi, J.E. Butler, S.H. Connell, B.P. Doyle, R.D. Maclear, J.P.F. Sellschop, E. Sideras-Haddad, D.B. Rebuli, Diamond Relat. Mater. 8 (1999) 1611.
[39] E.W. Plummer, T. Gustafsson, W. Gudat, D.E. Eastman, Phys. Rev. A 15 (1977) 2339.
[40] J. Shirafuji, T. Sugino, Diamond Relat. Mater. 5 (1996) 706.
[41] P. Gonon, A. Deneuville, E. Gheeraert, F. Fontaine, Diamond Relat. Mater. 3 (1994) 729.
[42] H. Kiyota, H. Okushi, T. Ando, M. Kamo, Y. Sato, Diamond Relat. Mater. 5 (1996) 718.
[43] W. Monch, Semiconductor Surfaces and Interfaces, Springer, Berlin, 1997, p. 113.
[44] K. Nakagawa, H. Nishimoto, Y. Enoki, S. Egashira, N. Ikenaga, T. Kobayashi, M. N-Gamo, T. Ando, T. Suzuki, Chem. Lett. 2001 (2001) 460.